

## RELATIVE TERRAIN IMAGING NAVIGATION (RETINA) TOOL FOR THE ASTEROID REDIRECT ROBOTIC MISSION (ARRM)

Cinnamon A. Wright\*, John Van Eepoel†, Andrew Liounis‡, Michael Shoemaker§, Keith DeWeese¶, Kenneth Getzandanner||

As a part of the NASA initiative to collect a boulder off of an asteroid and return it to Lunar orbit, the Satellite Servicing Capabilities Office (SSCO) and NASA GSFC are developing an on-board relative terrain imaging navigation algorithm for the Asteroid Redirect Robotic Mission (ARRM). After performing several fly-bys and dry runs to verify and refine the shape, spin, and gravity models and obtain centimeter level imagery, the spacecraft will descend to the surface of the asteroid to capture a boulder and return it to Lunar Orbit. The algorithm implements Stereophotoclinometry methods to register landmarks with images taken onboard the spacecraft, and use these measurements to estimate the position and orientation of the spacecraft with respect to the asteroid. This paper will present an overview of the ARRM GN&C system and concept of operations as well as a description of the algorithm and its implementation. These techniques will be demonstrated for the descent to the surface of the proposed asteroid of interest, 2008 EV5, and preliminary results will be shown.

### INTRODUCTION

NASA is developing the Asteroid Redirect Robotic Mission (ARRM) to capture a scientifically significant boulder from the surface of an asteroid, demonstrate a new planetary defense capability, and return the boulder to lunar orbit for astronauts to explore.<sup>1,2,3</sup> This previous work on the ARRM concept focused on asteroid Itokawa, to make use of previous survey data obtained from the Hayabusa mission. However the focus has now shifted to asteroid 2008 EV5 because EV5 is a carbonaceous chondrite which is of high interest to the scientific community, even though both satisfy the criteria for the desired launch date and mission duration. The target launch date for this mission is December 2020, with arrival at EV5 in October 2022, and return to Earth in late 2025. A representation of the vehicle and mission timeline are shown in Figure 1.

After launch, the outbound cruise to EV5 is performed with electric propulsion and takes approximately 15 months. Once in the vicinity of EV5, ARRM will survey and characterize the asteroid from ranges of 125 km to 25 km to map the surface, determine its spin state and refine the local gravity model. This global mapping phase will map the surface to an accuracy of 25 cm and require

\* Aerospace Engineer, Navigation and Mission Design Branch (Code 595), NASA Goddard Space Flight Center, Greenbelt MD, 20771, USA.

† Aerospace Engineer, Attitude Control Systems Engineering Branch, NASA Goddard Spaceflight Center, Greenbelt, MD 20771, USA.

‡ Pathways Intern, Navigation and Mission Design Branch (Code 595), NASA Goddard Space Flight Center, Greenbelt MD, 20771, USA.

§ Aerospace Engineer, a.i. Solutions, Inc., Lanham, MD, USA.

¶ Aerospace Engineer, Attitude Control Systems Engineering Branch, NASA Goddard Spaceflight Center, Greenbelt, MD 20771, USA.

|| Aerospace Engineer, Navigation and Mission Design Branch (Code 595), NASA Goddard Space Flight Center, Greenbelt MD, 20771, USA.

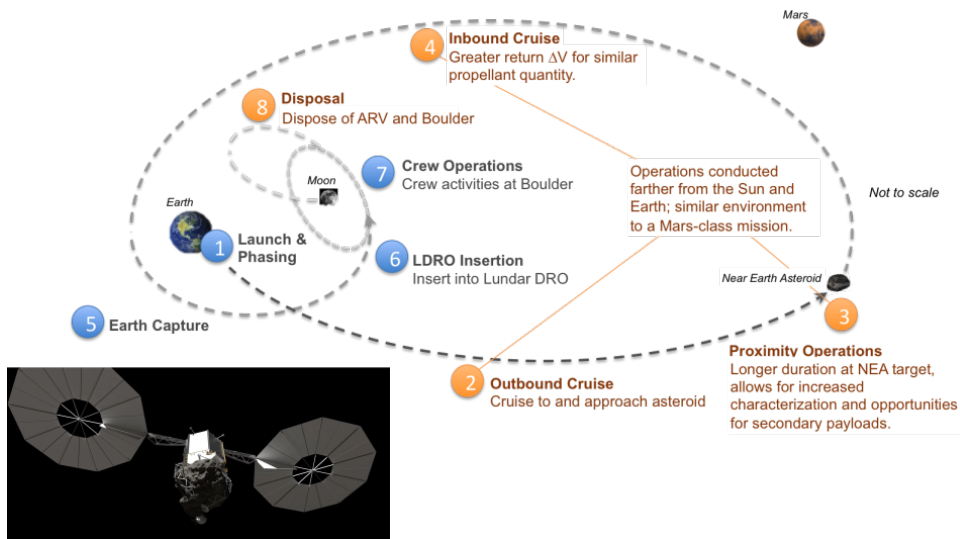


**Figure 1. ARM Concept of Operations with Vehicle Insert (lower left)**

43 days of imaging time. Analysis of this imagery will yield candidate landing sites of which more detailed survey imaging will be performed to obtain mapping accuracies to the 3 cm level. Upon completion of the survey, the ARRM vehicle returns to a hold point 5 km away from the asteroid. Analysis of the imagery by the ground will yield three candidate landing sites as well as an improved spin state, shape model and gravity model of EV5.

Maneuvers will be planned on the ground to transition the vehicle from 5 km to an altitude above the surface at 50 m, using a waypoint at 200 m above the surface. This begins the proximity operations phase<sup>2</sup> where the end result is to land on the asteroid. It is anticipated that on-board navigation will begin near the 1 km range to monitor the relative position of the vehicle with respect to the surface of EV5. After matching EV5's spin rate and beginning the descent at 50 m, the closed loop system takes control.

The ARRM system will utilize an architecture shown in Figure 2 to achieve navigation, maneuver planning and closed loop maneuver execution to land on the surface. The entire descent phase of the mission is completely autonomous, as is the boulder collection and ascent, and thus the navigation and control architecture must be robust. Once the boulder is retrieved and secured, the ARRM vehicle will insert into a halo orbit along the V-bar of the asteroid orbit for 260 days to perform a gravity tractor demonstration. After this activity, the ARRM vehicle, boulder and all, will head back to a lunar orbit for rendezvous with a human crewed vehicle.

ARRM will utilize Terrain Relative Navigation (TRN) to navigate to, and with enough precision, land over top of a boulder to enable extraction of the boulder off the surface. TRN is a method of estimating the relative state of a spacecraft to another body, such as a planet, moon, or asteroid using its natural topography. It is especially useful in navigating to bodies that are far away from Earth where other current measurement types, like DSN radiometric tracking, do not provide a measurement in the weak gravity fields that exist around asteroids and comets. In addition to the sensors used for TRN, a 3D LiDAR sensor will provide range to the surface, at a minimum; however, the discussion of this measurement type is outside the scope of this paper.

One of the most critical phases of the mission is the descent from 50 m to the surface of the asteroid. At touchdown, the spacecraft must be centered over the boulder with dispersions of less

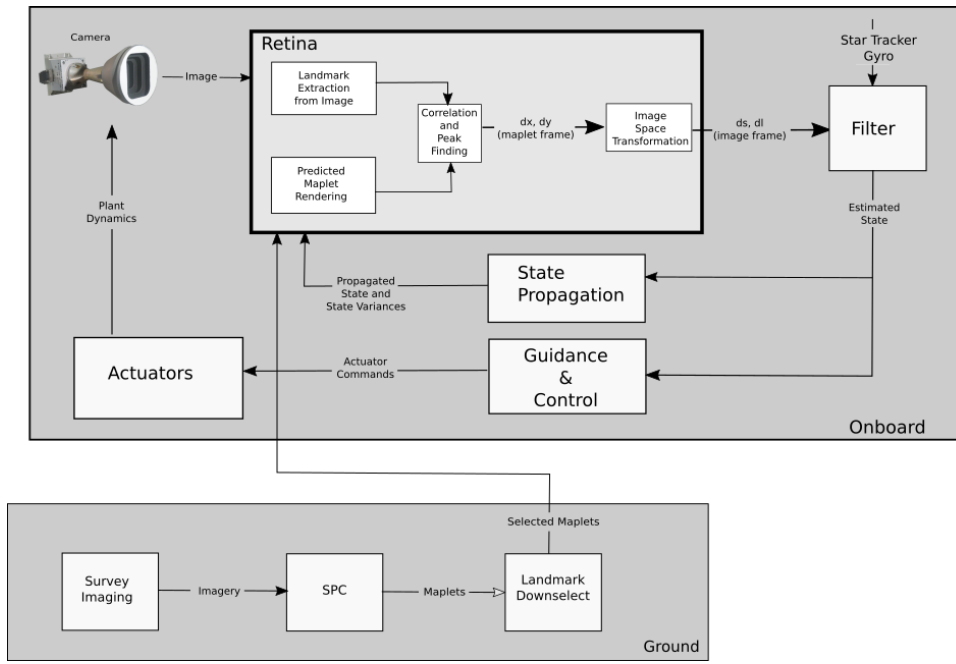


**Figure 2. ARRM Proximity Operations Guidance, Navigation and Control Diagram**

than 50 cm, lateral to the surface, to enable the robotic arms and gripper mechanisms to grasp the boulder. This paper will focus on the descent phase of the mission and present the methods for performing TRN, which we call Retina. Retina is derived from the stereophotoclinometry (SPC) methods developed by Gaskell,<sup>4</sup> which have a rich heritage on several small-body missions such as NEAR Shoemaker,<sup>5</sup> Hayabusa,<sup>6</sup> Rosetta,<sup>7,8</sup> Dawn,<sup>9</sup> and others.

Overall system performance for meeting ARRM requirements is not in the scope of this paper. This paper will focus on motivating particular elements of the Retina implementation, presenting details of the Retina components, and ending on a brief performance comparison between Retina and current ground-based TRN methods used for Origins-Spectral Interpretation-Resource Identification-Security-Regolith Explorer (OSIRIS-REx), known as SPC.

## IMPLEMENTATION MOTIVATION

Figure 2 outlines the elements needed by ARRM to navigate and control the spacecraft to land on the surface of an asteroid. This system includes a measurement, a filter, a guidance and control algorithm, and actuators to achieve closed loop control of the system. To properly motivate the design of the image processing and measurement generation process, Retina, the reader should have an understanding of the delineation of tasks in this closed loop system. The filter in this system would need to process several  $\Delta$ sample and  $\Delta$ line ( $\Delta s$ ,  $\Delta l$ ) measurements in a single image, as well as inertial information from the star trackers and gyros, to obtain position and velocity estimates relative to the asteroid fixed frame. Sample and line refers to the column and row of the detector array, respectively, and can be less than a whole pixel. Recall that through detailed surveys of the object, the relationship between the asteroid body fixed frame and the center of mass is known, and thus appropriate dynamics can be used in the filter. Figure 2 also shows that *State Propagation* is needed as input to Retina and that allows Retina to properly predict where landmarks in the image will appear and how far to search for them using the variance information from the filter. The use

of search distance will be discussed further in the next section.

Once a state estimate has been provided, the next step in closed loop control is to then determine how far from the goal the system is, known as guidance, and then to control to that error signal and actuate the system. This viewpoint of the closed loop control architecture is different than that shown in Reference 10, as that system had the filter and guidance embedded in the measurement system. Retina is a measurement only, and will produce several  $\Delta s$ ,  $\Delta l$  measurements from a single image, assuming the expected landmarks are visible in the image.

To complete the description of components in Figure 2, the ground elements use the imagery sent back to Earth and an *a-priori* shape model of the asteroid to build a higher resolution surface map. Currently, no change to the current state of the art system used for OSIRIS-REx, Rosetta, Dawn, Messenger, NEAR and others, is being considered to build these maps. From these maps, landmarks are extracted for use in the navigation process and in Retina.

The components in the Retina system start with identifying the area of pixels in the image that the landmark covers, identified in Figure 2 as *Landmark Extraction from Image*. This approach is different than current SPC methods being used where those missions projected the image data into the frame of the landmark.<sup>5,9</sup> This part of SPC requires several steps to ensure the image resolution was the same as the landmark, which could mean the averaging of pixel data. The next step is to render the landmarks in the image using the *a-priori* position and pointing information from the filter, as well as knowledge of the direction to the Sun.

Figure 3 provides a comparison of the landmark extracted from image data and the landmark rendered through current SPC methods described above. The predicted image in 3(b) shows a poor prediction in the shadowing of the surface because the method employed uses an approximation for shadowing. As such, the SPC processing must throw away much of this data when attempting to correlate the two images. Significant effort has gone into analyzing the performance of current SPC implementations,<sup>11</sup> and the conclusion was that the accuracy of the predicted image and the correlation peak location determination needed to be improved for ARRM.

In the ARRM concept of operations, the lighting angles that will occur will cause significant changes in shadow of the terrain due to the fast rotation rate of EV5 (3.725 h).<sup>12</sup> This, coupled with the tight dispersion requirements, has pushed the Retina algorithm to better predict this information that will be available in the image.

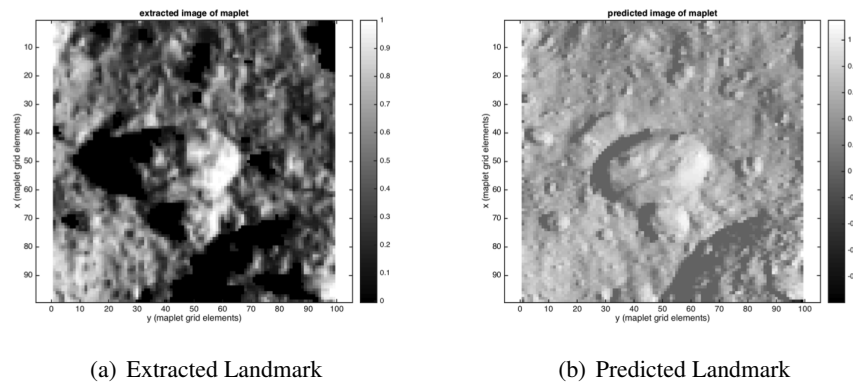


**Figure 3. SPC - applied to ARRM - Landmark in Image and Landmark Prediction**

The proposed resolution to shadow handling in current SPC systems is to instead render the landmark in the image space for on-board navigation by reflecting rays from the surface to the

camera. This problem can be made tractable on a flight embedded system through judicious use of acceleration methods and appropriate approximations of the lighting model. Figure 4 shows a comparison of the extracted and predicted landmark data using Retina. As can be seen the shadows and surface roughness are handled in a much more robust way, which allows the algorithm to be more robust overall.

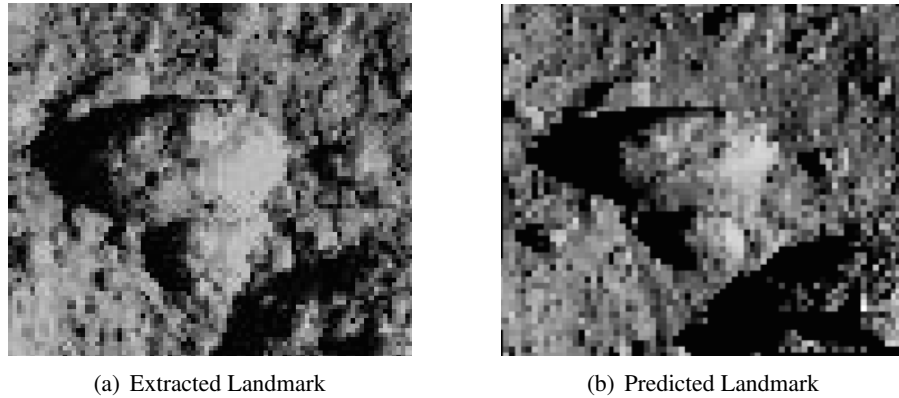


**Figure 4. Retina - applied to ARRM - Landmark in Image and Landmark Prediction**

Once the landmark has been rendered and the area in the image where the landmark should appear identified, the next step is to determine the correlation information over that area. Once the correlation matrix has been assembled, the peak of this correlation matrix must be found, which indicates a precise alignment of the predicted landmark information in the image. Significant analysis<sup>11</sup> uncovered a performance issue in determining the peak of the correlation matrix when applied to the ARRM scenario. Alternative methods were identified that improved the performance in the face of perturbations applied to the measurement process. The Retina approach incorporates these alternative methods, which are discussed in the next section.

## RETINA ALGORITHMS

The Retina implementation of TRN builds upon the ideas and methods of Dr. Robert Gaskell and his SPC approach<sup>5,13</sup>. The Retina implementation architecture seeks to improve upon the robustness and performance noted in the previous section. Figures 5 and 6 show the approach of generating measurements using landmark maps and images from a camera and a detailed processing flow diagram, respectively.

Recall that Figure 2 showed a *Ground* element that processes image data and generates maps of the surface and extracts landmark data. A subset of this landmark data, typically referred to as *maplets*, is selected on the ground based on the expected trajectory of the spacecraft and then uploaded, as depicted in Figure 5. With the landmark data in hand, Retina will use images from the camera along with the *a-priori* state information of the spacecraft to determine landmarks that should be visible in the image as well as generate predicted images of these landmarks. The predicted images will then be compared with the observed images to generate sample/line shifts between each observed/predicted pair, identifying the true location of each landmark in the image. Figure 6 shows an overview of this process. The following sections will go over each step in this process.

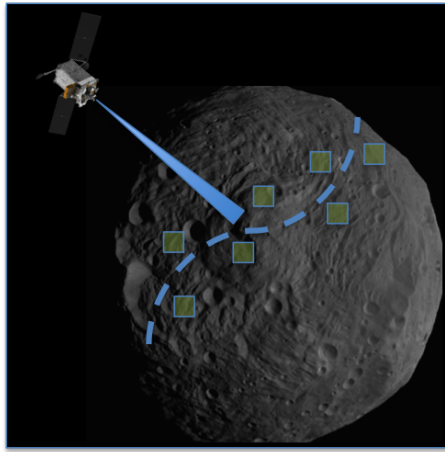


**Figure 5. Terrain Navigation Representation**

### Maplet Pre-Processing

The first phase in the Retina process is to load into memory the maplet data, which includes a digital elevation map (DEM) of relative heights, relative albedo data for each point of the model, body fixed location for the center of the maplet, and transformation information between the asteroid fixed frame and the DEM frame. The pre-processing of this data is to construct facets or triangle information from adjacent heights in the maplet data, which is a standard operation to tessellate a DEM. Delaunay Triangulation<sup>14</sup> is one method and generates a geometric representation suitable for intersection testing. Additional pre-processing of this triangulation is to compute the normals to the surface, which facilitate the intersection testing. All of this can be performed before any images are needed, and acceleration methods can be employed to aid the intersection testing to be done in *Landmark Prediction*, described in Figure 6.

### Maplet Projection Onto Image

In order to render the predicted image of the landmark, as shown in Figure 7, the *a-priori* knowledge of the spacecraft's state is combined with the knowledge of the asteroid's spin state and landmark locations to determine the predicted locations of the landmarks in the camera sensor frame. Using this information, the estimated pixel and line location of the landmark within the image can be computed using the pinhole camera model as shown in Figure 8.

The pinhole camera model attempts to describe how objects in three-dimensional space are projected onto a two-dimensional plane to form a photograph. It assumes that the world is being viewed through a pinhole, such that light travels in a straight path from the object, through the pinhole, and onto the focal plane of the camera. Thus, the pinhole camera model is actually just a simple gnomonic projection from  $\mathbb{R}^3$  to  $\mathbb{R}^2$ . In this section we briefly develop the pinhole camera model, loosely following the description in Hartley.<sup>15</sup>

To develop the mathematics behind the pinhole camera model, consider the scene in Figure 8. In the scene, we have a point,  $\mathbf{x}_B$  defined in frame  $B$ . We want to project this point onto the focal plane of the camera with focal length  $f$  and camera center located at  $\mathbf{t}_B$  in frame  $B$ . Our first step is to express  $\mathbf{x}_B$  in the camera frame (frame  $C$ ). We can do this using the simple rotation and translation given by

$$\mathbf{x}_C = \mathbf{T}_C^B (\mathbf{x}_B - \mathbf{t}_B) \quad (1)$$

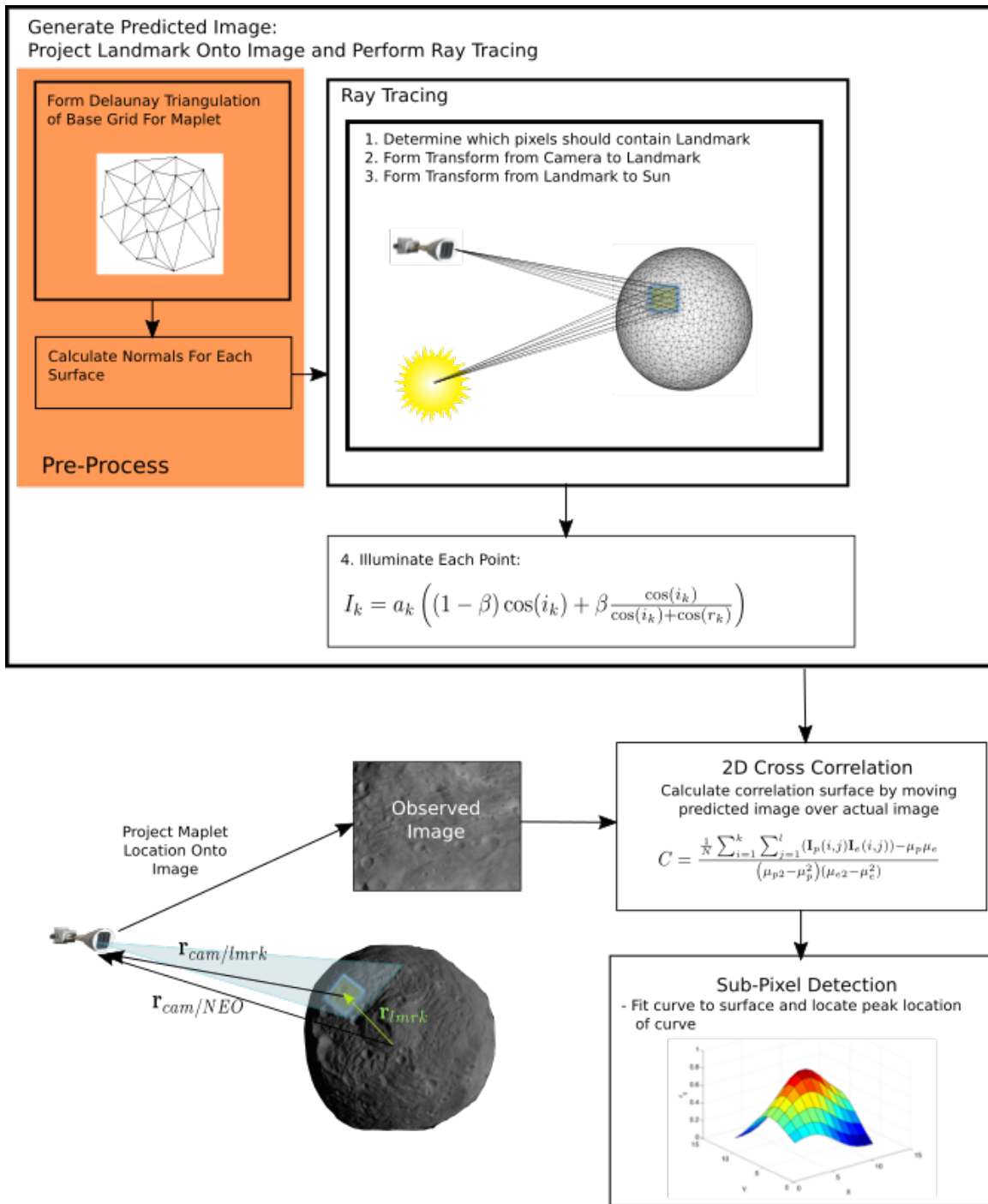


Figure 6. Retina Processing Flow Diagram

where  $\mathbf{x}_C$  is point  $\mathbf{x}_B$  expressed in the camera frame,  $\mathbf{t}_B$  is the location of the camera center (and origin of the camera frame) in frame  $B$ , and  $\mathbf{T}_C^B$  is a rotation matrix from frame  $B$  to the camera frame. Further, we can also express this transformation from frame  $B$  to frame  $C$  using homoge-

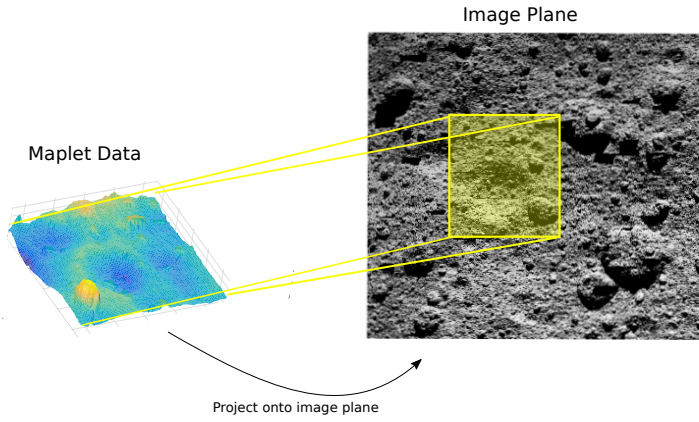


Figure 7. Landmark Projection onto Image Plane

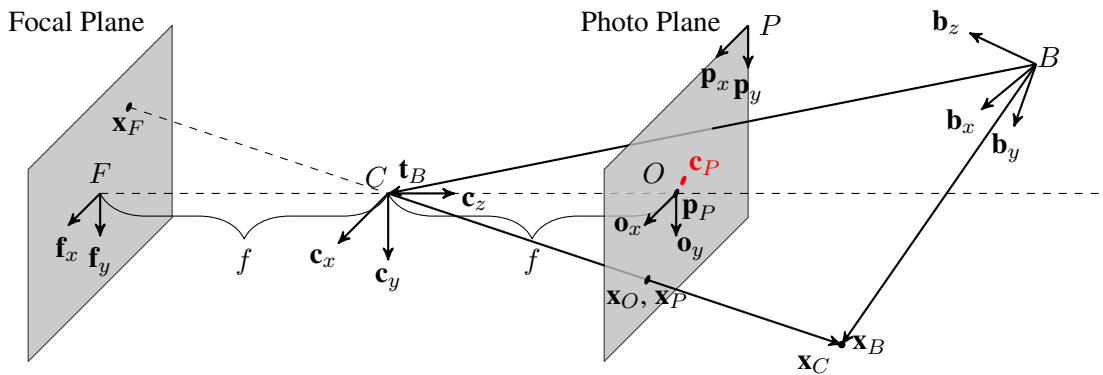


Figure 8. A point,  $\mathbf{x}_B$ , is projected onto the image plane through the pinhole camera model.

neous coordinates as

$$\mathbf{x}_C = \mathbf{T}_C^B \left[ \mathbf{I}_{3 \times 3} \mid -\mathbf{t}_B \right] (\mathbf{x}_h)_B = \mathbf{E}(\mathbf{x}_h)_B \quad (2)$$

where  $\mathbf{I}_{3 \times 3}$  is the  $3 \times 3$  identity matrix,  $(\mathbf{x}_h)_B$  is the homogeneous version of  $\mathbf{x}_B$ , and  $\mathbf{E} = \mathbf{T}_C^B \left[ \mathbf{I}_{3 \times 3} \mid -\mathbf{t}_B \right]$  is the extrinsic camera matrix (thus called because it is entirely dependent on the scene or external parameters).

Now that we have expressed our point of interest in the camera frame we can begin considering the projection. Start by examining the slice of the  $c_y$ - $c_z$  plane from Figure 8. To determine the  $y$ -coordinate of the point in the focal plane, we just need to multiply by the scaling term  $f/z_c$  and flip the sign to account for the fact that we have crossed the principal axis. This allows us to express the coordinates where the point projects onto the focal plane as follows:

$$\mathbf{x}_F = -\frac{f}{z_C} \begin{bmatrix} x_C \\ y_C \end{bmatrix} \quad (3)$$

where  $\mathbf{x}_F$  is the point expressed in the focal frame and  $f$  is the focal length of the camera expressed in units of pixels.

With the gnomonic projection in hand the points can be "distorted" through the use of a distortion

model<sup>16,17</sup> to approximate the effects of light distortion from the camera lens as well as manufacturing errors on the projection.

A distortion model is applied to get  $x_f$  and  $y_f$  and the coordinates are transformed to pixel,  $s$  and line,  $l$  coordinates as

$$\begin{pmatrix} s \\ l \end{pmatrix} = \begin{pmatrix} K_x & K_{xy} \\ K_{yx} & K_y \end{pmatrix} \begin{pmatrix} x_f \\ y_f \end{pmatrix} + \begin{pmatrix} s_o \\ l_o \end{pmatrix} \quad (4)$$

where the elements of  $\mathbf{K}$  have units equal to the reciprocal of the pixel dimensions.<sup>16</sup> This completes the mapping of a point in 3D space to a 2D point on the image plane through the pinhole camera model.

The portion of the image shown in Figure 7 is then compared with the predicted image, which is discussed in the next section. The above projection (along with its inverse) is extensively used throughout the Retina processes. The state covariance generated by the filter will be used to determine the search distance in the image in order to ensure that the area that is being correlated over actually contains the landmark while also attempting to minimize the correlation time required. These points must also be projected through this model to determine the appropriate search distance in the frame of the camera.

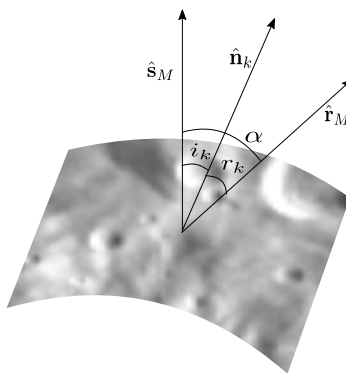


**Figure 9. Definition of Illumination Angles**

### Synthetic Image Generation

The ray tracing is performed by first identifying the corners bounding the area in the image occupied by the maplet according to the *a-priori* knowledge and camera model. Second, the pixels that cover the maplet are then taken through the inverse of the camera model in order to generate line of sight vectors out of the camera. Third, the intersection between these line of sight vectors and the faces of the triangular mesh of the maplet are calculated. Finally, the intersection points are then used as the starting points for rays directed toward the sun, which is used to check if the current point is shadowed or not. This is known as "single-bounce" ray tracing.<sup>18</sup>

After the ray tracing is complete each point is illuminated based on the McEwen illumination model,<sup>13</sup> with the definitions for the angles shown in Figure 9. For each intersection point that is not in shadow an illumination value is computed

$$I_k = a_k \left( (1 - \beta) \cos(i_k) + \beta \frac{\cos(i_k)}{\cos(i_k) + \cos(r_k)} \right) \quad (5)$$

where

$$\cos(i_k) = \hat{\mathbf{n}}_k^T \hat{\mathbf{s}}_M \quad (6)$$

$$\cos(r_k) = \hat{\mathbf{n}}_k^T \hat{\mathbf{r}}_M \quad (7)$$

$$\alpha = \cos^{-1}(\hat{\mathbf{s}}_M^T \hat{\mathbf{r}}_M), \quad (8)$$

and  $i_k$  is the incidence angle at location  $k$ ,  $r_k$  is the reflectance angle at location  $k$ ,  $\alpha$  is the phase angle,  $\hat{\mathbf{n}}_k$  is the local unit normal vector at triangle  $k$ ,  $\hat{\mathbf{s}}_M$  is the unit vector pointing in the direction from the surface feature to the sun expressed in the maplet frame, and  $\hat{\mathbf{r}}_M$  is the unit vector pointing in the direction from the surface feature to the camera expressed in the maplet frame. The term  $\beta = \exp(-\alpha/\alpha_0)$  is a weighting term used to approximate an appropriate mix of Lambertian and Lommel-Seeliger reflection models.<sup>13</sup>

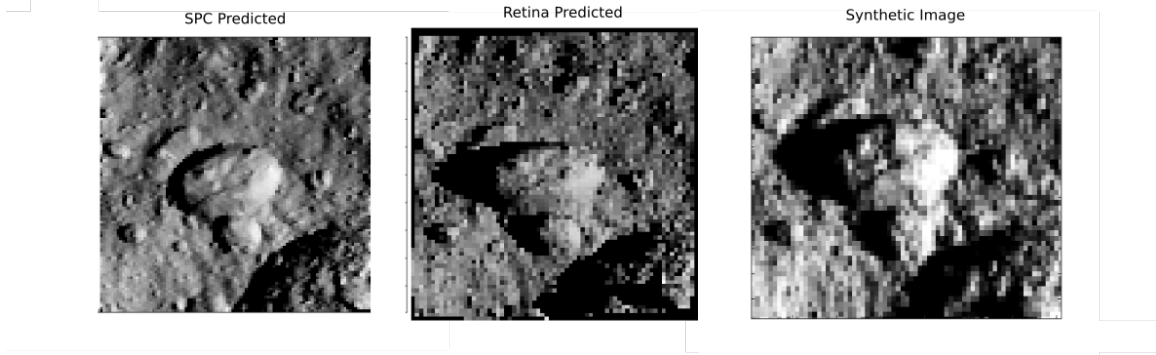


**Figure 10. Comparison of predicted images generated by the SPC process and Retina to synthetically generated image**

Figure 10 shows the rendering comparison between the SPC prediction method and Retina for the landmark mentioned in Figures 3 and 4. From this side by side comparison, the improvements in the Retina algorithm show more accurate shadows of the elevated terrain (rocks), as well as improved surface roughness that is not apparent in the SPC predicted image. The next section will attempt to quantify the improvement.

### Correlation Method

The correlation surface is calculated by shifting the predicted image over the actual image and computing the correlation coefficient given by

$$C = \frac{\frac{1}{N} \sum_{i=1}^k \sum_{j=1}^l (\mathbf{I}_p(i, j) \mathbf{I}_e(i, j)) - \mu_p \mu_e}{(\mu_{p^2} - \mu_p^2)(\mu_{e^2} - \mu_e^2)} \quad (9)$$

where  $C$  is the correlation value,  $N$  is the number of pixels that are nonzero in both the predicted and extracted images,  $I_p$  are the predicted illumination values, and  $I_e$  are the pixel values in the image, that both extend to row  $k$  and column  $l$ ;  $\mu_p$  and  $\mu_e$  are the average illumination values of the predicted and extracted pixels, and  $\mu_{p^2}$  and  $\mu_{e^2}$  are the average of the squares of the illumination values of the predicted and extracted pixels.<sup>19</sup>

## Peak Finding

In order to determine if there is any error between the predicted and extracted images, the peak value of the correlation surface must be determined. It is possible to determine the peak to sub-pixel accuracy by appropriately interpolating the surface around the correlation peak. Mentioned previously, the methods employed in current SPC implementations showed slightly biased results for the ARRM problem. To address this, a different interpolation approach was taken for Retina to minimize bias errors. A linear interpolation over a 3x3 sub-pixel grid is computed to find the peak in the correlation surface. This method, through significant analysis,<sup>11</sup> proved to perform the best with the ARRM descent scenario. Figure 11 provides the  $\Delta_{sample}$ ,  $\Delta_{line}$  error for correlating the images shown in Figure 10. This example problem did not perturb the image from the ideal location of the landmark, which should be in the center of the image.

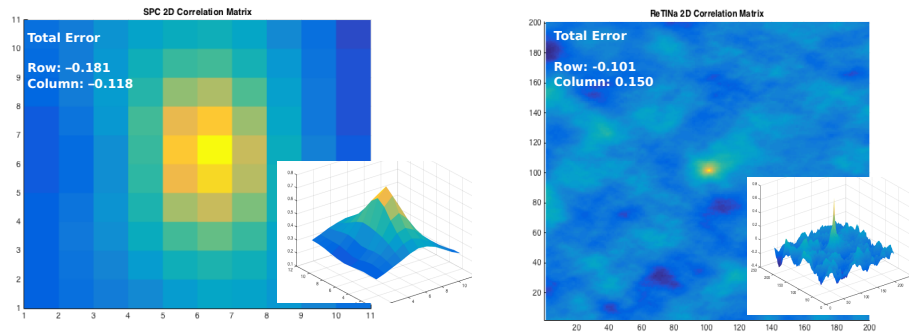


Figure 11. Comparison of correlation and peak finding methods.

## Final Output Phase

The final phase of output for the Retina algorithm is to ensure that all of the landmark measurements that it provides are consistent. This means that all of the computed shifts for all the landmarks should be in the same direction in the image plane. This computation is performed by determining the mean sample and line shifts for each measurement, and then comparing each measurement to this mean shift and flagging any outliers for the filter to handle appropriately.

## RETINA PERFORMANCE

The Retina algorithms described in previous sections were prototyped prior to implementation on an embedded system and the performance of this approach obtained. In this same system, the SPC algorithms were also implemented so as to obtain side by side comparisons of the two methods. The ARRM descent from 50 m was used as the profile for this analysis, and perturbations were applied to that trajectory and parameters consistent with the analysis presented in Ref. 17. This analysis also perturbed camera parameters, camera distortion parameters, landmark resolution, and direction to the Sun. The results are shown in Figure 12. The SPC implementation results in Figure 12(a) show a clear bias in its solutions, which can be attributed to approximations when rendering the landmarks for correlation. While the noise of the measurements appears lower, the SPC methods did not always return a result in many of the perturbation cases. The Retina implementation results in Figure 12(b) do not exhibit this same bias but do show slightly increased noise levels. Analysis of the results is on-going as the ARRM concept matures, but a preliminary observation during the

analysis shows that the Retina implementation is much more robust to perturbations in all quantities than the SPC implementation.<sup>11</sup>

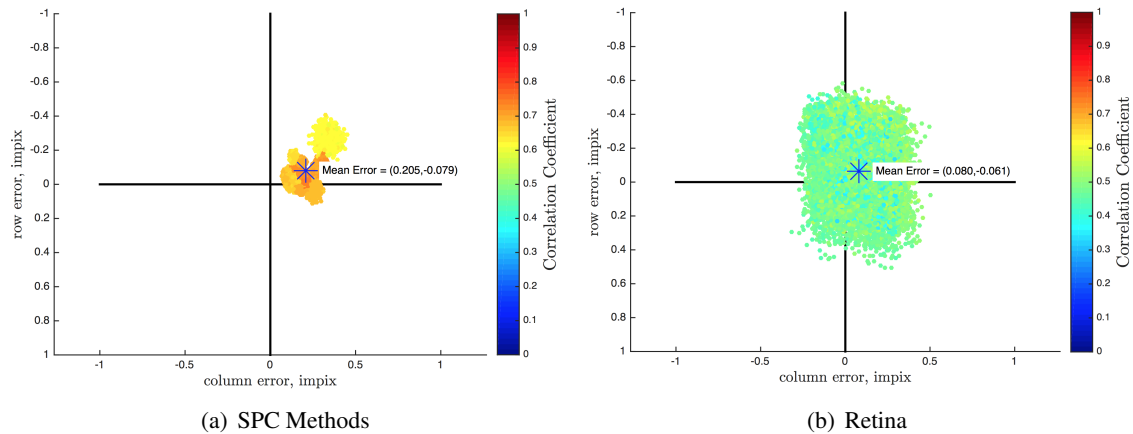


**Figure 12. Performance Comparison of Terrain Navigation Methods Applied to ARRMs Descent Scenario**

An initial implementation of the Retina algorithms described here have been implemented and executed on a flight-qualified embedded platform, SpaceCube.<sup>20,21</sup> This embedded system instantiates a Microblaze processor running at 75 MHz, and has 512 MB of DDR ram for access to the program being executed. The embedded system is running command and data handling software that consume 20% of the processor resources. The embedded system is set up to handle monochrome 1MP 10-bit image data at 3 Hz. The Retina implementation was tested on an initial test problem and results are promising that the implementation will run at the required update rate for ARRMs.

## CONCLUSIONS

This paper has presented an approach for performing terrain relative navigation to land on the surface of 2008 EV5, with a focus on the Retina measurement system, that will determine the location of landmarks in a sequence of images. The approach improves upon current state of the art methods being used for Dawn and OSIRIS-REx by improving the prediction of the landmark in the image, thereby improving the correlation of landmarks to the extracted image. The Retina implementation has been ported to an embedded platform and initial performance results have been obtained.

Future work will focus on additional testing and profiling of the implementation, identifying portions of the implementation that could be accelerated with either faster algorithmic implementations or through a hardware implementation. Additionally, work will also continue to assess the performance of the implementation against methods used by other NASA mission on other scenarios, and identifying improvements as necessary.

## ACKNOWLEDGMENTS

The authors would like to acknowledge the support of the Satellite Servicing Capabilities Office, Alex Pini of a.i. Solutions for his contributions for the ARRMs concept of operations information, Shaun Oborn and Reed McKenna of Solo Effects LLC for their development of the synthetic imagery renderer for asteroids, and finally to Steve Queen for being a valuable mentor and guide.

## REFERENCES

- [1] D. D. Mazanek, R. G. Merril, S. P. Belbin, D. M. Reeves, K. D. Earle, B. J. Naasz, and P. A. Abell, "Asteroid Redirect Robotic Mission: Robotic Boulder Capture Option Overview," *AIAA SPACE 2014 Conference and Exposition*, San Diego, CA, 2014.
- [2] D. M. Reeves, B. J. Naasz, C. A. Wright, and A. J. Pini, "Proximity Operations for the Robotic Boulder Capture Option for the Asteroid Redirect Mission," *AIAA SPACE 2014 Conference and Exposition*, San Diego, CA, 2014.
- [3] D. D. Mazanek, B. Naasz, B. Cichy, D. M. Reeves, and P. A. Abell, "Asteroid Redirect Mission Overview and Potential Science Opportunities," *European Planetary Science Congress 2015*, Feb. 2015, pp. vol 10, EPSC2015–279.
- [4] R. Gaskell *et al.*, "Characterizing and navigating small bodies with imaging data," *Meteoritics and Planetary Science*, Vol. 43, 2008, pp. 1049–1061.
- [5] R. W. Gaskell, "Optical Navigation Near Small Bodies," *AAS/AIAA Space Flight Mechanics Meeting*, San Diego, CA, Feb. 2011.
- [6] R. Gaskell, O. Barnouin-Jha, D. Scheeres, T. Mukai, N. Hirata, S. Abe, J. Saito, M. Ishiguro, T. Kubota, T. Hashimoto, J. Kawaguchi, M. Yoshikawa, K. Shirakawa, and T. Kominato, "Landmark Navigation Studies and Target Characterization in the Hayabusa Encounter with Itokawa," *AIAA/AAS Astrodynamics Specialist Conference and Exhibit, Keystone, Colorado*, 2006.
- [7] L. Jorda, P. L. Lamy, R. W. Gaskell, M. Kaasalainen, O. Groussin, S. Besse, and G. Faury, "Asteroid (2867) Steins: Shape, topography and global physical properties from OSIRIS observations," *Icarus*, Vol. 221, No. 2, 2012, pp. 1089–1100.
- [8] H. Sierks *et al.*, "On the nucleus structure and activity of comet 67P/Churyumov-Gerasimenko," *Science*, Vol. 347, No. 6220, 2015.
- [9] A. S. Konopliv, S. W. Asmar, R. S. Park, B. G. Bills, F. Centinello, A. B. Chamberlin, A. Ermakov, R. W. Gaskell, N. Rambaux, C. A. Raymond, C. T. Russell, D. E. Smith, P. Tricarico, and M. T. Zuber, "The Vesta gravity field, spin pole and rotation period, landmark positions, and ephemeris from the Dawn tracking and optical data," *Icarus*, Vol. 240, 2013, pp. 103–117.
- [10] Ryan Olds, Alexander May, Courtney Mario, Reid Hamilton, Chris Debrunner, and Kalle Anderson, "The Application of Optical Based Feature Tracking to OSIRIS-REx Asteroid Sample Collection," Breckenridge, CO, Feb. 2015.
- [11] M. A. Shoemaker, C. A. Wright, A. J. Liounis, K. M. Getzandanner, J. M. Van Eepoel, and K. D. DeWeese, "Performance Characterization of a Landmark Measurement System for ARRM Terrain Relative Navigation," *AAS Space Flight Mechanics Meeting*, Napa, CA, Feb. 2016.
- [12] M. W. Busch, S. J. Ostro, L. A. M. Benner, M. Brozovic, J. D. Giorgini, J. S. Jao, D. J. Scheeres, C. Magri, M. C. Nolan, E. S. Howell, P. A. Taylor, J.-L. Margot, and W. Briske, "Radar Observations and the Shape of Near-Earth Asteroid 2008 EV5," *Icarus* 212, 2011, pp. 649–660.
- [13] R. W. Gaskell, O. BARNOUIN-JHA, D. J. Scheeres, A. S. Konopliv, T. Mukai, S. Abe, J. Saito, M. Ishiguro, T. Kubota, T. Hashimoto, and others, "Characterizing and navigating small bodies with imaging data," *Meteoritics & Planetary Science*, Vol. 43, No. 6, 2008, pp. 1049–1061.
- [14] D.-T. Lee and B. J. Schachter, "Two algorithms for constructing a Delaunay triangulation," *International Journal of Computer & Information Sciences*, Vol. 9, No. 3, 1980, pp. 219–242.
- [15] R. Hartley and A. Zisserman, *Multiple View Geometry in Computer Vision*. Cambridge University Press, 2003.
- [16] W. M. Owen, "Methods of Optical Navigation," *AAS/AIAA Spaceflight Mechanics Meeting*, New Orleans, LA, Feb. 2011.
- [17] Cinnamon A. Wright, Sagar Bhatt, David C. Woffinden, Matthew Strube, Christopher D'Souza, and Keith DeWeese, "Linear Covariance Analysis For Proximity Operations Around Asteroid 2008 EV5," Breckenridge, CO, Feb. 2015.
- [18] A. Glassner, *An Introduction to Ray Tracing*. Morgan Kaufman Publishers, 1989.
- [19] J. P. Lewis, "Fast normalized cross-correlation," *Vision interface*, Vol. 10, 1995, pp. 120–123.
- [20] T. Flatley, "Advanced hybrid on-board science data processor - SpaceCube 2.0," *Earth Science Technology Forum*, 2010.
- [21] D. Petrick, A. Geist, M. Albaijes, M. Davis, P. Sparacino, G. Crum, R. Ripley, J. Boblitt, and T. Flatley, "SpaceCube v2.0 Space Flight Hybrid Reconfigurable Data Processing System," *Proceedings of the 2014 IEEE Aerospace Conference*, Big Sky, Montana, USA, 2014.